On the Origin of Dual Peak Phosphorescence and Ultralong Lifetime of 4,6-Diethoxy-2-carbazolyl-1,3,5-triazine

Lopa Paul,[a] *Swapan Chakrabarti,*[a,*] *and Kenneth Ruud.*[b,*]

[a]Department of Chemistry, University of Calcutta

92, A.P.C. Ray Road, Kolkata 700 009

India

[b]The Centre for Theoretical and Computational Chemistry

Department of Chemistry, UiT, The Arctic University of Norway

N-9037 Tromsø, Norway

AUTHOR INFORMATION

Corresponding Author

* E-mail: swapanchem@yahoo.co.in. Fax: 91-33-23519755

* E-mail: kenneth.ruud@uit.no.

ABSTRACT: Recently, ultralong phosphorescence lifetime has been observed in 4,6-Diethoxy-2-carbazolyl-1,3,5-triazine and H-aggregation induced stabilization of the T_1 state was suggested as its source. The response theory calculations demonstrate that the Davydov stabilization of the T_1 state of the dimer is marginal with respect to the monomer and the corresponding transition moments are virtually the same. Moreover, the calculated radiative rate constant is far from the experimental value, indicating that the ultralong lifetime is not likely to be of electronic origin only. Our calculations reveal that the dual peak emission from the T_1 state is due to strong vibronic coupling between the T_1 and S_0 state along selected normal modes. Interestingly, the calculated vibronic radiative rate constant of the dimer (2.33×10^{-3} s^{-1}) is comparable with the experimental value (4.7×10^{-3} s^{-1}), supporting the notion that vibronic contributions to the transition moment is responsible for the ultralong lifetime observed in the bulk system.

TOC GRAPHICS

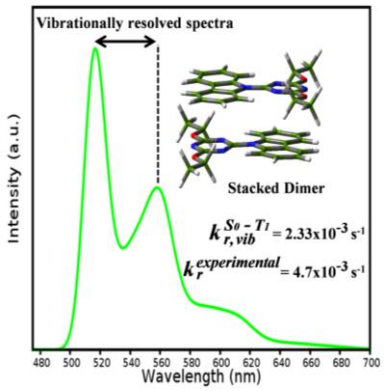

For centuries scientists have been trying to develop organic phosphorescent compounds, gradually increasing the efficiency of a wide array of optoelectronic applications, such as photovoltaics, photocatalytic reactions and molecular sensing.[1-3]Phosphorescence originates from the spin-forbidden radiative decay of excited triplet states to, in most cases, the singlet ground state, and is prone to non-radiative quenching and thus sensitive to high temperatures. To date, the progress made for organic phosphorescent compounds is far behind that of organic fluorescent materials.[4,5] This has spurred an interest in finding a protocol for the rational design of efficient organic phosphorescent materials. Historically, Lewis and Kasha first recognized the function of the triplet excited state and the significance of intersystem crossing (ISC) in phosphorescent molecules;[6] which they later in 1947confirmed to be the key parameters for phosphorescence in organic compounds.[7] Following these early works, several studies on organic molecules containing heavy atoms such as Br, I and functional groups such as the carbonyl moiety have demonstrated the possibility for ISC facilitating the phosphorescence process.[8-10] Recently, An *et al*.[11] synthesized simple organic molecules containing O, N, P that favored ISC. Their report suggested that H-aggregate dimers[12] (plane to plane stacked structures) effectively stabilize the triplet excited states, generating phosphorescence lifetimes of up to 1.35 s – several orders of magnitude longer than those of organic fluorophores.[13-14] However, they provided no explanation for why the studied organic phosphors show dual peak emissions and ultralong lifetimes for the T_1 state. Here we address these two fundamental issues associated with these organic phosphors in their H-aggregated form.

We consider 4,6-Diethoxy-2-carbazolyl-1,3,5-triazine (DECzT)[11] (Fig. 1) as it has the longest observed phosphorescence lifetime in the study of An *et al*.[11] Extensive computational analysis based on time-dependent density functional(TDDFT) response theory (RT)[15-17]calculations has

been carried out on the monomer and dimer of DECzT. To account for weak dispersion forces, the B97D[18] functional has been used in all calculations. The computation of the lifetime of both the monomer and the dimer has been done by evaluating the radiative rate constant (k_r)[19] and combined this with the experimentally observed non-radiative rate constant (k_{nr}).[11] Furthermore, we have inspected a variety of transition moments[19,20] , their vibronic contributions,[20] the nature of the orbitals involved in the phosphorescence process and calculated the components of the spin-orbit coupling (SOC)[21,22] constant, in sum providing insight into the origin of the ultralong phosphorescent lifetime[23,24] of this system.

The geometries of the monomer and dimer were optimized using the dispersion-corrected B97D functional in combination with the 6-311G(d,p) basis set (Figure 1) using the Gaussian 09 program[25]. In case of the dimer, both the parallel and anti-parallel orientations of the donor and acceptor moieties were considered. The energy difference between the parallel and anti-parallel configurations was found to be small (~ 0.01eV). For consistency with the work of An *et al.*[11], we use the anti-parallel configuration for all TDDFT calculations. The planarity of the structures is preserved both for the monomer and the dimer of DECzT. The optimized structure of the dimer of DECzT in its ground state has a stacking distance of 3.17 Å, (Figure 1).

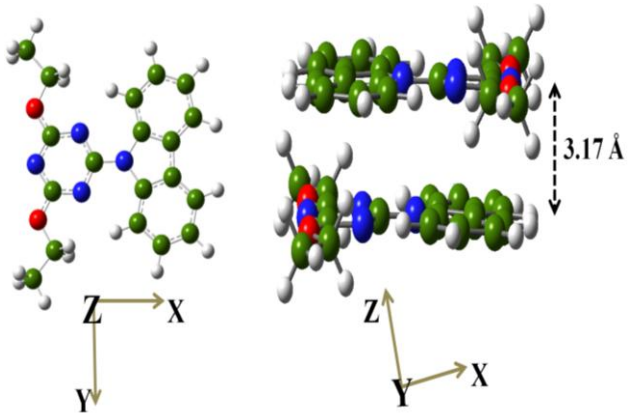

Figure 1. Optimized geometry of DECzT in the ground state – monomer (left), dimer (right).

To probe the spectral properties of the optimized monomer and dimer, TDDFT calculations were conducted using B97D with the cc-pVDZ basis set. The calculated one-photon absorption (OPA) parameters obtained for the excitation from the electronic ground state (S_0) to the excited state for which the oscillator strength is the largest (S_n) for the monomer and dimer together with the experimental excitation wavelength reported by An *et al.*[11] are presented in Table S1 of the Supporting Information. A detailed discussion of the corresponding orbital pair contributions is given in Section 2 of the Supporting Information. The absorption spectra for both the monomer and dimer of DECzT are shown in Figure 2a. The strongest absorption of the DECzT-monomer occurs at a wavelength of 325.7 nm and corresponds to the $S_0 \rightarrow S_2$ transition. Our calculated absorption wavelength for the strongest absorption band of the dimer is 326.5 nm and corresponds to the $S_0 \rightarrow S_8$ transition. The experimentally reported value[11] for the absorption wavelength of H-aggregated DECzT is 365 nm.

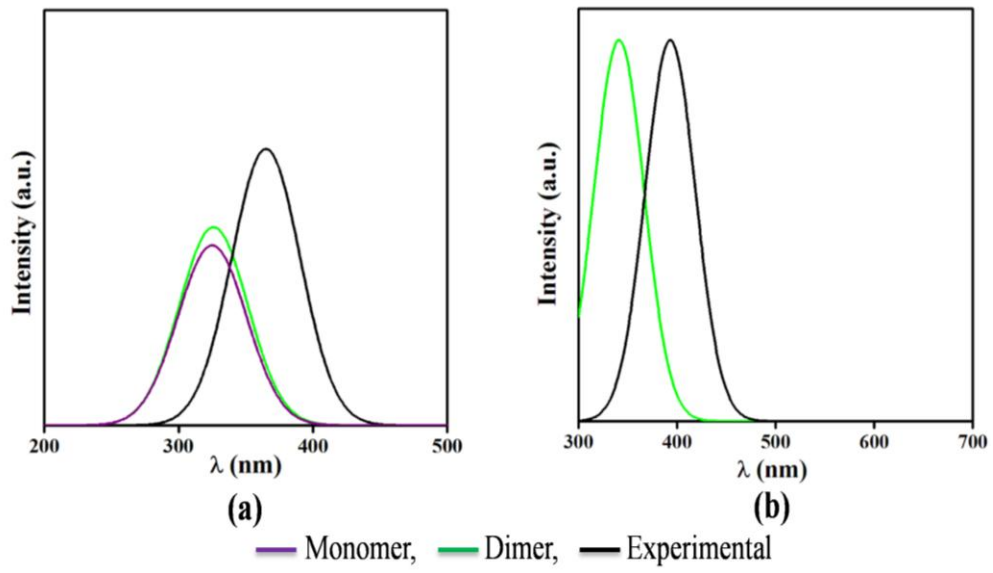

Figure 2. Spectra (FWHM = 60 nm) of DECzT (a) absorption and (b) fluorescence.

The molecular orbitals (MO) involved in the excitation process in the dimer (Figure S1 and Table S1, Supporting Information) clearly shows that the excitation has a mixed charge-transfer (CT) and π-electron density reorganization character, whereas it for the monomer (Figure S1, Supporting Information) only involves a reorganization of the π-electron density for this HOMO (H) → LUMO (L) transition.

It is well known that transitions to higher excited states $S_0 \rightarrow S_{1+n}$ may occur, as also is the case in our calculations. However, Kasha's rule[26] ensures a quick relaxation to S_1, making it the most relevant state for which to study the excited-state properties. To support the use of Kasha's rule, we computed the energy differences between the S_1 and the relevant S_n states. The energy differences are small enough (<1eV) to suggest that they facilitate a rapid internal conversion (IC) from the S_n state to the final S_1 state. The emission (fluorescence) spectrum for the dimer is depicted in Figure 2b as the monomer does not emit in the visible range (~350 – 700 nm). The computed fluorescence parameters of the dimer together with the major contributing molecular orbitals are presented in Table S2 of the Supporting Information. The dimer shows a peak near the UV region at 341.1 nm, whereas the experimental spectra display an emission band at 393 nm (Figure 2b).

In order to understand the details of the phosphorescence mechanism in both the monomer and dimer of DECzT, we need to identify the possible ISC channels. For the monomer, the T_4 state is about 0.1 eV above the S_1 state and involves same orbital composition as that of S_1, making it a good channel for ISC. Moreover, the spin-orbit coupling (SOC) between S_1 and T_4 ($< S_1| H_{SO} | T_4>$) is 0.043 cm^{-1}. Although T_3 also lies close in energy to the S_1 state, its orbital composition does not match well with the S_1state, and the correspondingly low SOC ($< S_1| H_{SO} | T_3>$=0.0001 cm^{-1}) value reduces the probability for ISC from this state. As seen from scheme 1, due to rapid

vibrational relaxation (VR), the T_3 state decays to the T_1state, and finally leads to the observed phosphorescence. In the dimer, the triplet states T_1-T_4 lies within a narrow energy region. The SOC between S_1 and T_1($< S_1| H_{SO} | T_1>$) and S_1 and T_3($< S_1| H_{SO} | T_3>$) are 0.092 and 0.063 cm^{-1}, respectively and they involve same orbitals as in theS_1state and thus provides a possible route for ISC, although also in the case of the dimer, T_3 will undergo VR and finally reach $T_1$from which phosphorescence will occur.

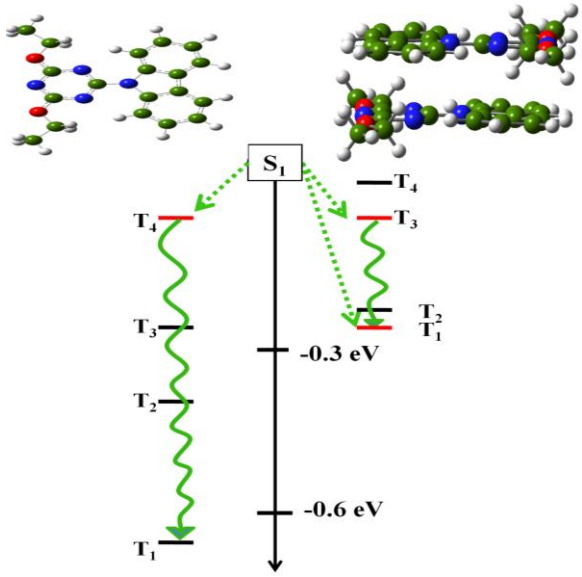

Scheme1. Probable transition channels for ISC in monomer (left) and dimer (right) of DECzT.

The experimental phosphorescence spectrum of DECzT[11] was recorded at room temperature, having two peaks at 529 nm and at 574 nm, respectively. The TDDFT response theory predicts that theT_1 emission of the monomer will occur at 506 nm whereas it is red-shifted to 515 nm for the dimer. This indicates that the T_1 state of the dimer is only stabilized by 0.05 eV relative to monomer. The calculations further reveal that T_1 emission wavelength of the tetramer (537 nm) is in very good agreement with the experimental value, indicating that the cooperative effect vis-à-vis Davydov stabilization[27] of the T_1 state has little influence on the phosphorescence

wavelength corresponding to the first peak of the H-aggregated system. Note that the phosphorescence wavelength does not change significantly upon addition of diffuse functions in the basis set.

To understand the nature of the phosphorescence process, we have calculated the Λ parameter,[28] which measures the degree of spatial overlap between the moduli of all pairs of occupied and virtual orbitals involved in a specific electronic transition, at the B97D/cc-pVDZ level of theory. The value of Λ ranges between 0 and 1. The greater the value of Λ, the larger is the spatial overlap between the occupied and virtual orbitals, suggesting that the electronic transition does not lead to a significant shift in the electron density. The Λ values of the monomer is 0.76, whereas it for the dimer it is 0.73. Phosphorescence transitions thus have short-range intramolecular CT character as is evident from the nature of the orbitals involved in the transition process as shown in Figure 3.

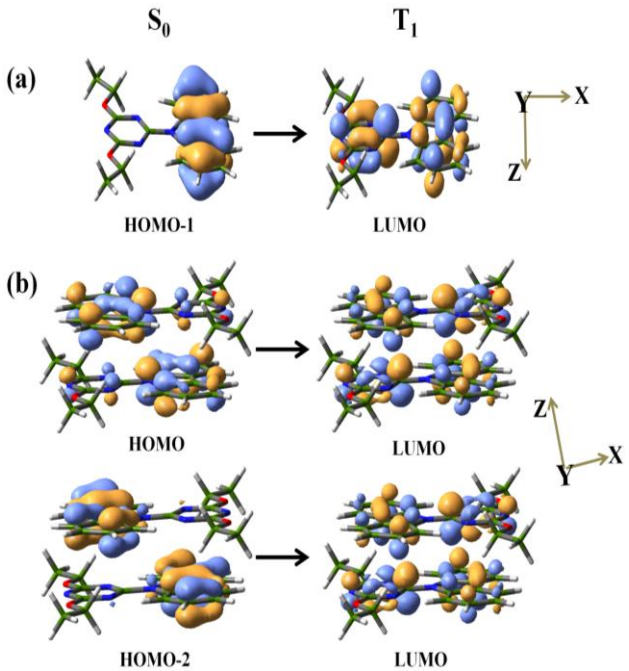

Figure 3. Molecular orbitals showing transition in triplet states of DECzT (a) monomer (isovalue = 0.04) and (b) dimer (isovalue = 0.04).

We have also computed the radiative rate constant for the $T_1 \rightarrow S_0$ transition ($k_r^{S_0\text{-}T_1}$) in the high temperature limit where all the zero-field split components of the T_1 state contribute to the net phosphorescence process. The radiative rate constant can be calculated using[19]

$$k_r^{S_0\text{-}T_1} = \frac{4\alpha_0^3}{3\,t_0}\omega_{S_0\text{-}T_1}^3 \sum_{i\in(x,y,z)} \left|M^i_{S_0\text{-}T_1}\right|^2 \; and \; \tau = \frac{1}{k_r^{S_0\text{-}T_1} + k_{nr}} \qquad \textbf{(1)}$$

where α_0 is the fine-structure constant, $t_0 = (4\pi\varepsilon_0)^2\hbar^3/m_e e^4$ in a.u., $\omega_{S_0\text{-}T_1}$ is the transition energy between the ground state (S_0) and the final triplet states (T_1) expressed in cm^{-1}, k_{nr} is the non-radiative rate constant, $M^i_{S_0\text{-}T_1}$ is the spin-orbit coupled S_0-T_1 phosphorescence transition moment in a.u. and τ is the lifetime in seconds. The expression for $M^i_{S_0\text{-}T_1}$ is

$$M^i_{S_0-T_1} = \sum_{n=0}^{\infty} \frac{\langle S_0|\hat{\mu}_i|S_n\rangle\langle S_n|\hat{H}_{SO}|T_1\rangle}{E(S_n)-E(T_1)} + \sum_{m=1}^{\infty} \frac{\langle S_0|\hat{H}_{SO}|T_m\rangle\langle T_m|\hat{\mu}_i|T_1\rangle}{E(S_0)-E(T_m)} \qquad \textbf{(2)}$$

where $\hat{\mu}_i$ and $\hat{H}_{SO}$ are the dipole and spin-orbit operators, respectively. S_n and T_m are the intermediate singlet and triplet states with T_1 as the final triplet state. It is important to mention here that the sum-over-states (SOS) approach is computationally expensive, and for this reason we have used density functional quadratic response theory for evaluating the components of $M^i_{S_0\text{-}T_1}$ and the spin-orbit coupling constant of the T_1 and S_0 states. In all calculations, the full one- and two-electron Breit-Pauli SO-integrals has been used, as implemented in Dalton[29,30].

The net electronic contribution to the phosphorescence transition moments of the monomer and dimer are 9.68 x 10^{-5} and 9.80 x 10^{-5} a.u, respectively. Using the above expression, the corresponding $k_r^{S_0-T_1}$ values are found to be 3.71 x 10^{-2} and 3.58 x 10^{-2} s^{-1}, respectively, and these values are approximately eight times larger than that of experiment. The large discrepancy between the experimentally observed radiative rate constant (4.7 x10^{-3} s^{-1}) and the theoretically predicted values combined with the dual peak emission feature of T_1 suggests that the mechanism of the phosphorescence process in this system does not originate solely from the electronic contribution as proposed by An *et al.*[11]. The experimental gap between the two peaks is quite small (0.18 eV) and as a result, the two peaks may represent a vibrational progression of the T_1 emission.

In order to include vibronic effects in our calculations, we used the approach of Ruhoff *et al.*[31] as implemented in ADF 2016[32]. In this approach, the normal modes of the triplet states (T_1) are expressed as $Q^{T_1}=\mathbf{J}Q^{S_0}+\mathbf{k}$ where **J** is the Duschinsky rotation matrix and **k** is a displacement vector. The Franck-Condon (FC) overlap integral between the vibrational wave functions of the T_1 and S_0 states is then computed by evaluating the integral, $S(\nu';\nu) = \det(\mathbf{J})^{-1/2}\int\psi'(\nu')\,\psi(\nu)\,dQ$.

With this approach, the vibrational progression of the T_1 emission of the monomer and dimer are simulated and for comparison, the experimentally observed spectrum of the bulk system and the simulated spectrum for the dimer is shown in Figure 4.

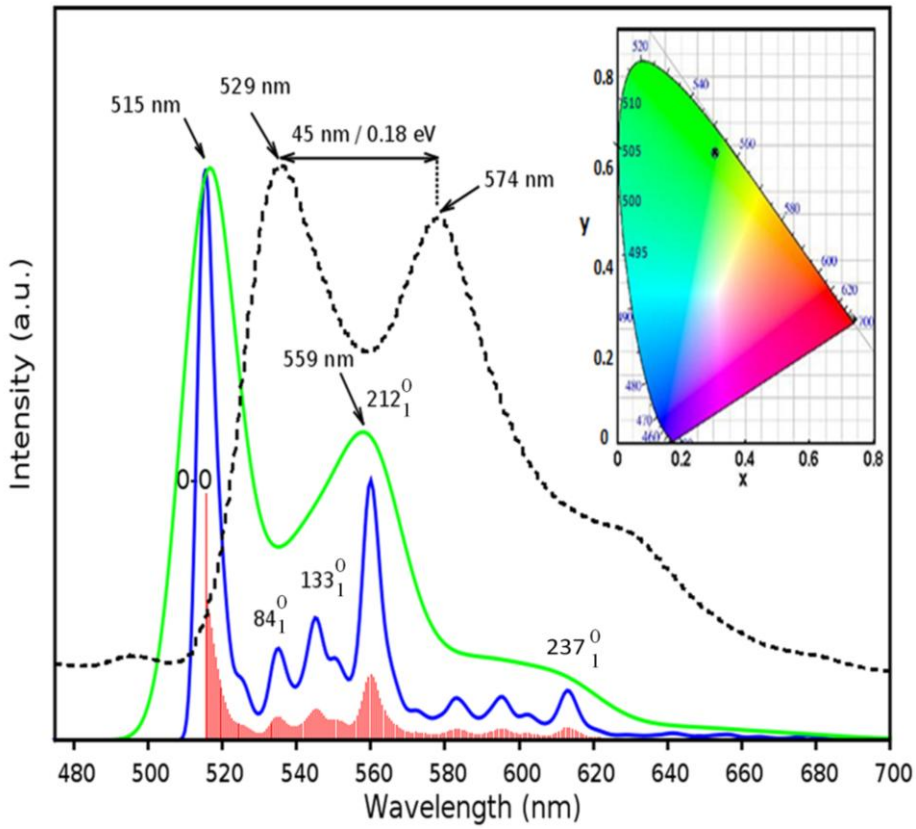

Figure 4. Simulated Franck-Condon $T_1 \rightarrow S_0$ phosphorescence emission spectra of DECzT-dimer is shown by solid lines, (—) and (—) represents the calculated spectra with constant FWHM =100cm^{-1} and 600 cm^{-1} respectively. The four most active vibrational modes together with the 0-0 band are considered. (·····) denotes the experimental spectra. Red lines represent the stick diagram of the emission spectrum. The calculated CIE-1931 coordinates (black dot) for DECzT-dimer are also shown.

The vibrationally resolved phosphorescence spectrum of the monomer is presented as Figure S2 in the Supporting Information. We have presented the simulated phosphorescence spectrum using two different values for the full width at half maximum (FWHM), namely 100 and 600 cm^{-1}. The simulated spectrum with higher FWHM resembles quite well the experimental spectrum recorded at room temperature. It is evident from Figure 4 that the two peaks of the dimer appear

at 515 and 560 nm. The separation between the two peaks is 0.19 eV, whereas the experimental gap is 0.18 eV. This excellent agreement between experiment and theory strongly suggests that these peaks are indeed vibrational components of the T_1 emission. The inset in Figure 4 represents the CIE-1931color space chromaticity diagram, and the simulated color of the dimer is the same as that of the bulk material, indicating that the dimer gives a good representation of the emission processes in the bulk material. It is also worth noting that the color of the monomer (yellow) is different from that of the bulk/dimer. To gain additional insight into the vibronic couplings, we have inspected the normal modes of vibration of the two states carefully. The lower wavelength peak represents the 0-0 transition whereas the second major peak comes from the vibronic coupling involving a specific normal mode coupling the two states. The calculations reveal that the frequency of this particular normal mode of the dimer is 1557 $cm^{-1}$and involves the in-plane bending motion of the carbazolyl-moiety. Apart from this normal mode, three other modes, though to a lesser extent, are also contributing, which is evident from the simulated spectrum with lower FWHM and the corresponding mode frequencies are 704 cm^{-1}, 1050 cm^{-1} and 3109 cm^{-1}. The four modes with their displacement vectors are shown in Figure 5.

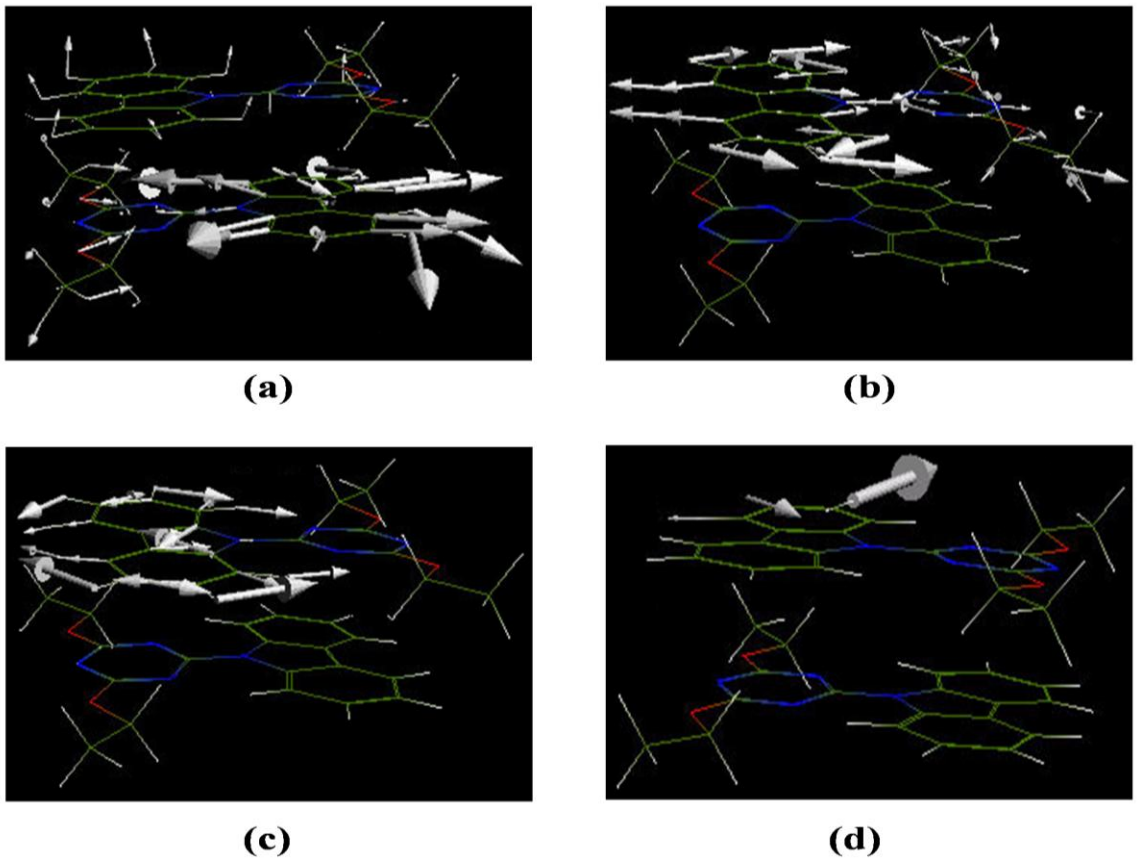

Figure 5. Displacement vector of the contributing vibrational modes of DECzT-dimer (a) ν_α= 704 cm^{-1} displaying stretching and out of plane bending of mainly carbazolyl group, (b) ν_α= 1050 cm^{-1}showing scissoring motion of the carbazolyl moiety and bending cum stretching of triazine part, (c) ν_α= 1557 cm^{-1} reveals in plane bending of carbazolyl group and (d) ν_α= 3109 cm^{-1} having asymmetric C-H stretching in carbazolyl moiety.

It has been found that the 0-0 FC overlap integral ($S_{0\text{-}0}$) of the monomer (0.28) is much higher than that of the dimer (0.017). The $S_{0\text{-}0}$-weighted transition moment of monomer and dimer is 2.71 x 10^{-5} and 1.69 x 10^{-6} a.u, respectively. The transition moments computed from the electronic contribution alone and with the $S_{0\text{-}0}$-weighted one along with their corresponding radiative rate constants are presented in Table S3 of the Supporting Information. With these new transition moments, the calculated radiative rate constants of the monomer and dimer are 3.04 x

10^{-3} s^{-1} and 1.07 x 10^{-5} s^{-1}, which shows that the radiative rate constant of the dimer is more than 400 times smaller than the experimental value (4.7 x 10^{-3} s^{-1}), albeit the spectral feature of the bulk material is essentially reproduced at the dimer level. It has previously been shown that the incorporation of the $S_{0\text{-}0}$ term alone cannot explain the intensity of the vibronic phosphorescence band of benzene.[20] In principle, the transition moment of a vibronic phosphorescence band can be written as:[20,33]

$$M_{S,T}^{\nu',\nu} = M_{S,T}^{\nu'\nu}(Q_0)\int \chi_{S,\nu'}\chi_{T,\nu}\,dQ + \eta_\alpha \int \chi_{S,\nu'}Q_\alpha \chi_{T,\nu}\,dQ \qquad \textbf{(3)}$$

where ν and ν' represent vibrational states of the T_1 and S_0states, which in our case are 0 and 1 respectively, $\chi_{S,\nu'}$and $\chi_{T,\nu}$ are vibrational wave functions and $\eta_\alpha = \delta/\delta Q_\alpha\,([M_{S,T}(Q)]_{Q_0=0})$. The first term represents the transition moment of the 0-0 band at a given nuclear configuration and the second term gives the nuclear displacement-induced transition moments for the 0-1 band associated with different normal modes of vibration (α). According to Minaev et al,[20] the contribution of the second term involving all the 0-1 bands in the high temperature limit will appear in the radiative rate constant as follows:

$$k_{r,vib}^{S_0\text{-}T_1} = \frac{1}{\tau} = \frac{4}{3x137^3}\omega_{S_0\text{-}T_1}^3 \sum_\alpha \left|\eta_\alpha\right|^2 \; 2\pi\nu_\alpha \qquad \textbf{(4)}$$

ν_α is the corresponding frequency for the α vibrational mode, the factor 1/137 represents the value of the fine-structure constant in a.u. and the other terms have been defined previously. To evaluate η_α, we first computed the transition moments of the dimer with a displacement of ±0.02 a.u. along the contributing normal modes and then performed a numerical vector differentiation. For simplicity, we have only considered 0-1 bands. The contribution of $|\eta_\alpha|^2 2\pi\nu_\alpha$ term in the vibronic radiative rate constant for each of the significant normal modes is presented in Table 1.

Table 1: Vibrational modes, first derivative of transition moments [η_α (a.u.)], frequencies [v_α (a.u.)], vibrational component induced corresponding radiative rate constant [$k_{r,vib}^{S_0\text{-}T_1}$ (s^{-1})] and experimentally observed radiative rate constant [$k_r^{experimental}$ (s^{-1})] of DECzT-dimer.

DECzT	**Frequency modes (α)**	$\lvert\eta_\alpha\rvert$	v_α	$\lvert\eta_\alpha\rvert^2 2\pi v_\alpha$	$k_{r,vib}^{S_0 - T_1}$	$k_r^{experimental}$
Dimer	84	$6.7158\text{x}10^{-5}$	$3.23\text{x}10^{-3}$	$0.9148\text{x}10^{-10}$	$2.33\text{x}10^{-3}$	$4.7\text{x}10^{-3}$
	133	$7.9211\text{x}10^{-5}$	$4.82\text{x}10^{-3}$	$1.8992\text{x}10^{-10}$		
	212	$8.4267\text{x}10^{-5}$	$7.16\text{x}10^{-3}$	$3.1929\text{x}10^{-10}$		
	237	$1.3659\text{x}10^{-5}$	$1.41\text{x}10^{-2}$	$0.1652\text{x}10^{-10}$		

Table 1 suggests that the net vibronic contribution to the rate constant is 2.33×10^{-3} s^{-1} which is fairly close to the experimentally estimated radiative rate constant value. The corresponding radiative rate constant of the monomer is more than ten times higher. In the present context, if we accept the experimental value of the non-radiative constant (0.78 s^{-1}), the calculated observed lifetime will be 1.28 s in excellent, and likely fortuitous, agreement with experiment of 1.28 s,[11] indicating that the displacement-induced vibronic transition moment has profound impact on the ultralong lifetime of the system studied here. In summary, our analysis suggests that the origin of the ultralong lifetime of the H-aggregated organic phosphor is a molecular phenomenon.

To conclude, our calculations have shown that the dual peak phosphorescence spectrum of DECzT originates from the strong vibronic coupling between selected normal modes coupling the S_0 and T_1 states. The experimental gap (0.18 eV) between the peaks is in excellent agreement with the theoretically predicted gap of 0.19 eV for the dimer. However, the Franck-Condon overlap-weighted phosphorescence transition moment fails to reproduce the radiative

rate constant. To rationalize the observed ultralong lifetime of the H-aggregated phosphor molecule, we have investigated the vibrationally induced phosphorescence transition moment for the 0-1 band of selected normal modes and have found that the vibronic phosphorescence transition moment actually plays a key role in determining the value of the radiative rate constant. The calculated vibronic radiative rate constant (2.33×10^{-3} s^{-1}) corroborates nicely with the experimental value (4.7×10^{-3} s^{-1}). Finally, the phophorescence spectral features along with the ultralong lifetime of DECzT appears to be satisfactorily converged at the dimer level, giving additional support to the notion that the observed photo-physics of the bulk system is governed by vibronic coupling at the molecular level.

ASSOCIATED CONTENT

Supporting Information.

(1) Computational details. (2) Co-ordinates of the optimized geometry of DECzT in both dimeric and monomeric forms. (3) OPA parameters. (4) Fluorescence parameters. (5) Vibrationally resolved phosphorescence spectrum of the DECzT-monomer. (6) Pure electronic and S0-0 weighted transition moment. (7) Vibrational frequencies of monomer and dimer of DECzT. The Supporting information is available free of charge. (PDF)

AUTHOR INFORMATION

Notes

The authors declare no competing financial interests.

ACKNOWLEDGMENT

L.P. thanks K.R. for his hospitality during her visit to the CTCC. L.P. also thanks the Council of Scientific and Industrial Research (CSIR) for granting her the Junior Research Fellowship.

REFERENCES

(1) Bakulin, A. A. *et al*. The Role of Driving Energy and Delocalized States for Charge Separation in Organic Semiconductors. *Science* **2012**, *335*, 1340-1344.

(2) Xing, G. C. *et al*. Long-Range Balanced Electron and Hole-Transport Lengths in Organic-Inorganic $CH_3NH_3PbI_3$. *Science* **2013**, *342*, 344-347.

(3) Garcia-Garibay, M. A. Advances at the Frontiers of Photochemical Sciences. *J. Am. Chem. Soc.* **2012**, *134*, 8289-8292.

(4) Uoyama, H.; Goushi, K.; Shizu, K.; Nomura, H.; Adachi, C. Highly Efficient Organic Light-Emitting Diodes from Delayed Fluorescence. *Nature* **2012**, *492*, 234–238.

(5) Jankus, V.; Chiang, C. -J.; Dias. F.; Monkman, A. P. Deep Blue Exciplex Organic Light-Emitting Diodes with Enhanced Efficiency; P-type or E-type Triplet Conversion to Singlet Excitons? *Adv. Mater*. **2013**, *25*, 1455–1459.

(6) Lewis, G. N.; Kasha, M. Phosphorescence and the Triplet State. *J. Am. Chem. Soc.* **1944**, *66*, 2100–2116.

(7) Kasha, M. Phosphorescence and the Role of the Triplet State in the Electronic Excitation of Complex Molecules. *Chem. Rev.* **1947**, *41*, 401–419.

(8) Winnik, M. A.; Lemire, A.; Lee, C. K.; Saunders, D. S. The Phosphorescence of Substituted Benzophenones in Solution: Effects of Polar and Protic Solvents on Hydrocarbon Chain Conformation. *J. Am. Chem. Soc.* **1976**, *98*, 2000–2002.

(9) Winnik, M. A.; Basu, S. N.; Lee, C. K.; Saunders, D. S. The Phosphorescence of Substituted Benzophenones in Solution: A Probe of Hydrocarbon Chain Conformation in Three Non-polar Solvents. *J. Am. Chem. Soc.* **1976**, *98*, 2928–2935.

(10) Hurtubise, R. J. Phosphorimetry. *Anal. Chem*. **1983**, *55*, 669–680.

(11) An, Z.; Zheng, C.; Tao. Y.; Chen, R.; Shi, H.; Chen, T.; Wang, Z.; Li, H.; Deng, R.; Liu. X.; Huang, W. Stabilizing Triplet Excited States for Ultralong Organic Phosphorescence. *Nat. Mater.* **2015**, *14*, 685-690.

(12) Spano, F. C.; Silva, C. H- and J-Aggregate Behavior in Polymeric Semiconductors. *Ann. Rev. of Phys. Chem.* **2014**, *65*, 477-500.

(13) Baldo, M. A.; O'Brien, D. F.; You, Y.; Shoustikov, A.; Sibley, S.; Thompson, M. E.; Forrest, S. R. Highly Efficient Phosphorescent Emission from Organic Electroluminescent Devices. *Nature* **1998**, *395*, 151-154.

(14) Lakowicz, J. R. *Principles of Fluorescence Spectroscopy*; Springer: New York, USA, 2006.

(15) Hattema, H.; Jensen, H. J. Aa.; Jørgensen, P.; Olsen, J. Quadratic Response Functions for a Multiconfigurational Self-Consistent Field Wave Functions. *J. Chem. Phys.* **1992**, *97*, 1174-1190.

(16) Runge, E.; Gross, E. K. U. Density-Functional Theory for Time-Dependent Systems. *Phys. Rev. Lett.* **1984**, *52*, 997-1000.

(17) Salek, P.; Vahtras, O.; Helgaker, T.; Ågren, H. Density-functional Theory of Linear and Nonlinear Time-Dependent Molecular Properties. *J. Chem. Phys.* **2002**, *117*, 9630-9645.

(18) Grimme, S.; Ehrlich, S.; Goerigk, L. Effect of the Damping Function in Dispersion Corrected Density Functional Theory. *J. Comp. Chem.* **2011**, *32*, 1456-1465.

(19) Younker, J. M.; Dobbs, K. D. Correlating Experimental Photophysical Properties of Iridium (III) Complexes to Spin-Orbit Coupled TDDFT Predictions. *J. Phys. Chem.* **2013**, 117, 25714-25723.

(20) Minaev, B. F.; Knuts, S.; Ågren, H.; Vahtras, O. The Vibronically Induced Phosphorescence in Benzene. *Chemical Physics* **1993**, *175*, 245-254.

(21) Vahtras, O.; Ågren, H.; Jørgensen. P.; Jensen, H. J. A.; Helgaker, T.; Olsen, J. Spin-orbit Coupling Constants in a Multiconfiguration Linear Response Approach. *J. Chem. Phys.* **1992**, *96*, 2118-2126.

(22) Manchon, A.; Koo, H. C.; Nitta, J.; Frolov, S. M.; Duine, R. A. New Perspectives for Rashba Spin–Orbit Coupling. *Nature Mater.* **2015**, *14*, 871-882.

(23) Gill, R.; Tian, L.; Amerongen, H. V.; Subramaniam, V. Emission Enhancement and Lifetime Modification of Phosphorescence on Silver Nanoparticle Aggregates. *Phys. Chem. Chem. Phys.* **2013**, *15*, 15734-15739.

(24) Kühn, M.; Weigend, F. Phosphorescence Lifetimes of Organic Light-Emitting Diodes from Two-Component Time-Dependent Density Functional Theory. *J. Chem. Phys.* **2014**, *141*, 224302.

(25) GAUSSIAN 09, revision D.01, Gaussian, Inc., Wallingford, CT, 2009.

(26) Kasha, M. Characterization of Electronic Transitions in Complex Molecules. *Disc. Faraday Soc.* **1950**, *9*, 14-19.

(27) Datta, A.; Pati, S. K. Intermolecular Interactions in Supramolecular Aggregates: Understanding Cooperative Phenomena for Nonlinear Optical Responses. *Chem. Soc. Rev.* **2006**, *35*, 1305-1323.

(28) Vahtras, O.; Ågren, H.; Jørgensen. P.; Jensen, H. J. A.; Helgaker, T.; Olsen, J. Multiconfigurational Quadratic Response Functions for Singlet and Triplet Perturbations: The Phosphorescence Lifetime of Formaldehyde. *J. Chem. Phys.* **1992**, *97*, 9178-9187.

(29) Tunell, I.; Rinkevicius, Z.; Vahtras, O.; Trygve, P. S.; Ågren, H. Density Functional Theory of Nonlinear Triplet Response Properties with Applications to Phosphorescence. *J. Chem. Phys.* **2003**, *119*, 11024-11034.

(30) DALTON, a Molecular Electronic Structure Program; Release Dalton2016.2 (2015), see http://daltonprogram.org.

(31) Ruhoff, P. T.; Ratner, M. A. Algorithms for Computing Franck-Condon Overlap Integrals. *International journal of Quantum Chemistry* **2000**, *77*, 383-392.

(32) ADF2016, SCM, Theoretical Chemistry, Virje Universiteit, Amsterdam, The Netherlands, http://www.scm.com.

(33) Löwdin, P. O. *Advances in Qunatum Chemistry*; Elsevier: California, USA, 1996.